Effects of injection strategy on performance and emissions metrics in a diesel/methane dual-fuel single-cylinder compression ignition engine

Metin Korkmaz[1] (iD), Dennis Ritter[2], Bernhard Jochim[1], Joachim Beeckmann[1], Dirk Abel[2] and Heinz Pitsch[1]

Abstract

In order to counteract the drawbacks of conventional diesel combustion, which can lead to high indicated specific nitric oxide and indicated specific particulate matter emissions, a promising diesel-dual-fuel concept is investigated and evaluated. In this study, methane is used as supplement to liquid diesel fuel due to its benefits like high knock resistance and clean combustion. A deep understanding of the in-cylinder process is required for engine design and combustion controller development. To investigate the impact of different input parameters such as injection duration, injection timing, and substitution rate on varying output parameters like load, combustion phasing, and engine-out emissions, numerous investigations were conducted. Engine speed, global equivalence ratio, and injection pressure were held constant. The experiments were carried out in a modified single-cylinder compression ignition engine. The results reveal regimes with different dependencies between injection timing of diesel fuel and combustion phasing. This work demonstrates the potential of the diesel-dual-fuel concept by combining sophisticated combustion control with the favorable combustion mode. Without employing exhaust gas recirculation, TIER IMO 3 emissions limits are met while ensuring high thermal efficiency.

Introduction

The compression ignition (CI) engine is widely used in heavy-duty as well as in light-duty applications due to its higher efficiency enabled by high compression ratios, short combustion duration, and un-throttled air operation.[1,2] In conventional diesel combustion (CDC), high-reactivity fuels like diesel fuel are injected close to top dead center (TDC) initiating mixing-controlled combustion. This diffusion combustion leads to high emissions of indicated specific nitric oxide ($ISNO_x$) and indicated specific particulate matter (ISPM, soot) due to locally slightly lean and very rich areas as well as high local peak temperatures. $ISNO_x$ and ISPM have negative impact on the environment and human respiratory diseases[3,4] and hence are governmentally regulated. In order to meet the strict emissions legislations, exhaust after-treatment devices are required for modern CI engines. These devices can lead to higher fuel consumption, reduced engine performance, increased cost and complexity, and often require additional agents, like urea.[4–7] Therefore, research efforts have been focused on the minimization of engine-out emissions, the maximization of overall engine efficiency, and the reduction of dependency on exhaust after-treatment devices.[4]

[1]Institute for Combustion Technology, RWTH Aachen University, Aachen, Germany
[2]Institute of Automatic Control, RWTH Aachen University, Aachen, Germany

Corresponding author:
Metin Korkmaz, Institute for Combustion Technology, RWTH Aachen University, Templergraben 64, 52056 Aachen, Germany.
Email: m.korkmaz@itv.rwth-aachen.de

To achieve this goal, advanced combustion strategies with in-cylinder $ISNO_x$ and ISPM reduction methods are required.[6] The low-temperature-combustion (LTC) concept is one promising concept due to its potential of simultaneous reduction of $ISNO_x$ and ISPM, because of lower peak temperatures and increased homogeneity. Recent research results as well as detailed overviews on LTC are given in previous works.[8–12]

Another approach to counteract the drawbacks of CI engines is the utilization of alternative fuels, which is referred to as diesel-dual-fuel (DDF) concept, that is, the combination of two fuels with different auto-ignition characteristics. For example, the introduction of low-reactivity fuel into the intake air, promoting a homogeneous gas/air mixture that is compressed rapidly, with the direct injection of high-reactivity fuel, which triggers the ignition, has been found to be a promising solution.[13,14] The use of natural gas as a supplementary fuel is beneficial due to its availability, widespread distribution infrastructure, low cost, high auto-ignition temperature, and clean-burning qualities.[14] Furthermore, proven reserves of natural gas are significantly larger than those of crude oil.[15] For more details on dual-fuel and recent research results, the reader is referred to previous works.[4–7,10,13,14,16–27]

The main component of natural gas is methane (e.g. 92 vol% quoted in Huang and Crookes[28]), which is the simplest hydrocarbon fuel and has the highest H/C ratio among all petroleum-derived fuels. Thus, the combustion of methane is cleaner and emits less CO_2.[14] The addition of natural gas to the intake air results in an increased overall heat capacity and therefore lowering the combustion temperature. This consequently leads to lower $ISNO_x$ emissions in comparison to CDC. Moreover, soot emissions in DDF engines are very low due to prolonged ignition delay time and reduced amount of diesel fuel.[14,15,29–32] For the DDF operation, significantly higher amounts of indicated specific total hydrocarbons (ISTHC) were reported. The increase in ISTHC can be attributed to lean mixture and low temperature in the combustion chamber. Thus, the combustion is not propagating throughout the charge. Moreover, the trapped mass in the crevices is not ignited because of the low temperature in the expansion stroke.[14] The high amount of ISTHC emissions are the main drawback and limiting factor of DDF operation due to low catalyst conversion efficiencies for CH_4.[14,23]

To analyze the high emissions of ISTHC, Königsson et al.[23] conducted experiments in a single-cylinder engine for five different pistons with varying top land geometries. The top land volume was identified as the main source of ISTHC emissions for a certain range of fuel-air ratio (Φ). Moreover, it was shown that a reduction in the top land volume led to a decrease in the ISTHC emissions. Srinivasan et al.[33] investigated the effect of intake charge temperature and pilot injected quantity on the performance and emissions on a single-cylinder engine. Improvements in combustion

performance, stability, and emission for low load were reported. Königsson et al.[22] conducted experiments on a single-cylinder engine with variations in Φ, from the stoichiometric to the lean limit, for different load points. In addition, the impact of inlet temperature, diesel pilot quantity, EGR-rate, and CA50 sweeps were studied. The use of a cost-effective exhaust after-treatment system was enabled by the combination of high EGR rates and increased inlet air temperature. Zhou et al.[34] investigated the impact of diesel injection timing and the diesel pilot mass on the combustion and emission metrics in a single-cylinder engine. A reduction of the pollutant emissions for appropriately advancing the diesel fuel injection timings was reported. In order to explore the effects of natural gas injection timing on combustion performance, Yang et al.[35] investigated two different pilot injection timings and injection pressures for various injection timings of natural gas. The results showed that the pilot injection parameters, like injection pressure and timing, and natural gas injection timing have a significant effect on the combustion performance and emissions. While delayed natural gas injection timings improved engine performance at low load, a better brake thermal efficiency was achieved by higher injection pressures and advanced injection timings. To summarize, based on the discussion above, the injection timing and the amount of the injected diesel are the key parameters in a DDF engine. Moreover, the combustion mode in DDF operation is a function of the substitution rate (SR), defined as the percentage of the energy of the high-reactivity fuel, which is replaced by the low-reactivity fuel. At low SR, the combustion is dominated by diffusion, while with increasing SR, the combustion mode transitions to a combination of diffusion and deflagration. For high SR, a small premixed combustion of the high-reactivity fuel initiates the deflagration of the gas/air mixture.[19]

For the successful development of the efficient DDF combustion process, knowledge of the process characteristics is required. Thus, the objective of this study is to investigate and evaluate the impact of the dual-fuel key parameters (injection timing, injection duration, and SR) on the combustion phasing. The engine is operated with premixed methane/air mixture, that is, methane is injected after the surge tank, and pilot injection of diesel fuel. Engine speed, global equivalence ratio, and injection pressure are held constant. These data are meant to support the development of a model-based combustion controller, which can adjust the desired load, the combustion phasing, and the SR at the same time. Thus, the goal is to ensure stable dual-fuel operation for the considered load range under stationary and transient conditions with flexible SRs.

This article is arranged as follows: the experimental setup is described in section "Experimental setup," while section "Methodology" explains the methodology underlying this work. In section "Experimental results," the results of the stationary engine operation for different SR are presented and discussed. Finally, the major

Table 1. Engine and injector specifications.

Quantity	Value	Unit
Displaced volume	390	ccm
Stroke	88.3	mm
Bore	75.0	mm
Compression ratio	15.1:1	–
Number of cylinders	1	–
Valves per cylinder	4	–
Swirl number	1.386	–
Nozzle	6-hole	–
Included spray angle	120	°

findings and the conclusions from this study are summarized.

Experimental setup

Experiments in this study were carried out in a single-cylinder research engine. It has an overall displacement of 0.390 L, with bore and stroke of 75 and 88.3 mm, respectively. For the DDF investigations, the compression ratio was reduced from 17.4:1 to 15.1:1.

A high-pressure, common-rail fuel injection system (electronically controlled) with maximum injection pressure of 1600 bar is used for the diesel injection. A centrally located solenoid injector with six equally spaced orifices with nominal diameters of 0.142 mm is utilized. An overview of engine and injector specifications is given in Table 1.

In Figure 1, the schematic test bench layout is illustrated. The air supply was ensured by a three-stage supercharger unit consisting of three EATON M62 compressors with intercoolers and a maximum absolute pressure of 3.4 bar. For heating the inlet air, an external heater was utilized. Furthermore, auxiliary systems for heating or cooling oil, water, and fuel were applied to the test bench in order to maintain well-defined conditions. The load was represented by a DC engine equipped with a torque meter.

For controlling the engine (i.e. intake pressure, exhaust pressure, injection timing, duration, and pressure), a customized engine control unit (ECU) was used. A dSPACE rapid prototyping controller (RCP) hardware (MicroAutobox 2) was integrated into the engine control system. The control methods were developed in Simulink and executed on the RCP hardware. The communication with the customized ECU was ensured by the use of the by-pass function of the ECU.

Intake airflow was determined by an ABB Sensyflow FMT-700P unit. Inlet and exhaust temperatures were measured with k-type thermocouples, while piezoresistive absolute pressure sensors from Kistler, that is, inlet sensor (4005BA5FA2) in conjunction with amplifier (4618A2) and exhaust sensor (4075A10) combined with amplifier (4618A0), were adapted to the engine. Furthermore, the injection pressure for the diesel fuel was metered with a piezoresistive high-pressure sensor (4067A2000A2) and an amplifier (4618A2). For the analysis of in-cylinder parameters, for example, indicated mean effective pressure of the high-pressure process ($IMEP_{HP}$), CA50, and heat release rate (HRR), a piezoelectric pressure sensor (6056AS42) is mounted via a glow plug adapter into the combustion chamber. The measured charge is amplified (5011B) and converted to a proportional voltage output signal, which was evaluated in a thermodynamic real-time analysis module (TRA) from Ingenieurgesellschaft Auto und Verkehr (IAV). The pressure trace was metered with an accurate resolution of 0.2 °CA and averaged over 100 consecutive cycles. The high resolution of the crankshaft was ensured by an encoder from AVL (365C).

Gaseous engine-out emissions were measured by ABB exhaust gas analyzers including THC (Fidas 24), O_2 (Magnos 206), CO, and CO_2 (Uras 26). NO, NO_2, and NO_x emissions were measured via Ecophysics CLD 700el. The exhaust gas was collected by a heated probe (180 °C) in the exhaust pipe. In addition, particulate matter (PM) measurements were performed with AVL Micro Soot Sensor 483. For combustion controller development as well as transient engine operation, emissions of THC and NO_x were measured with HFR 500 fast FID and CLD 500 fast NO_x, respectively. Table 2 summarizes the measured species, the
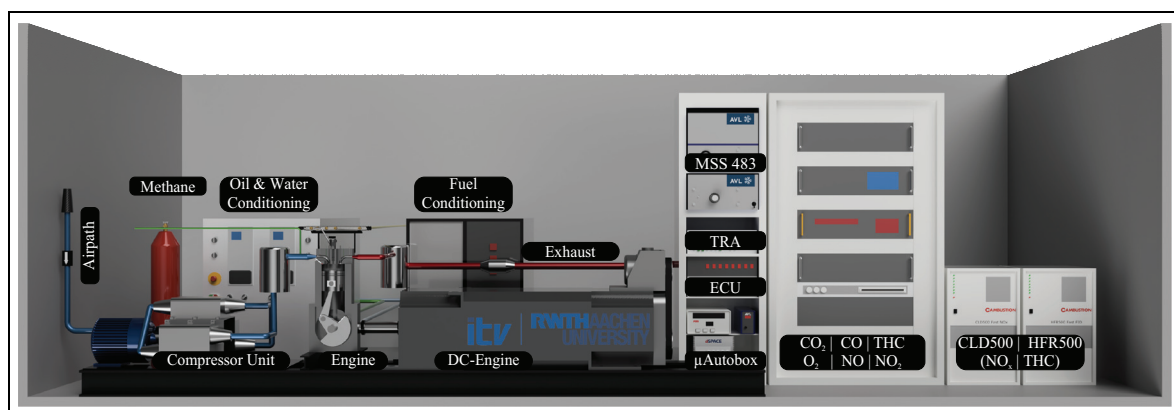

Figure 1. Schematic test bench layout.

Table 2. Measured species, measuring methods and accuracy (full scale, FS) of the devices.

Species	Method	Accuracy
NO/NO$_x$	CLD	$\leqslant \pm 1.0\%$ FS
NO/NO$_x$ (fast)	CLD	$\leqslant \pm 1.0\%$ FS
THC	FID	$\leqslant \pm 0.5\%$ FS
THC (fast)	FID	$\leqslant \pm 1.0\%$ FS
CO	Infrared-photometer	$\leqslant \pm 0.5\%$ FS
CO$_2$	Infrared-photometer	$\leqslant \pm 0.5\%$ FS
O$_2$	Magneto-mechanical	$\leqslant 50$ ppm

CLD: chemiluminescence detection; FID: flame ionization detector; THC: total hydrocarbons.

Table 3. Diesel fuel (CEC RF-06-099) properties.

Quantity	Method	Value	Unit
Cetane number	EN ISO 5165	53.1	–
Density at 15 °C	ISO 3675	834.5	kg/m^3
Sulfur content	ASTM D5453	< 10	ppm
Net heating value	ASTM D3338	43.203	MJ/kg
H/C Ratio	ASTM D3343	1.89	mol/mol
Dist. 50%	EN ISO 3405	270.7	°C
Dist. 95%	EN ISO 3405	346.2	°C
Dist. FBP	EN ISO 3405	362.3	°C
Viscosity at 40 °C	EN ISO 3104	2.934	mm^2/s

FBP: final boiling point.

measuring methods, and the accuracy of the devices. The ECM EGR 5230 module performed simultaneous measurements of air-fuel ratio (AFR) and external exhaust gas recirculation (EGR) rate.

In this study, a high purity European reference diesel (cf. Table 3) was used as the high-reactivity fuel and CH$_4$ with a purity of 99.5% as low-reactivity fuel, respectively. Diesel fuel was directly injected into the combustion chamber, while CH$_4$ was injected into the airflow, that is, after the surge tank. The injection pressure was set to 5 bar and the injection quantity was adjusted by a mass flow controller (MCP-50SLPM-D) from Alicat Scientific.

Methodology

Experimental approach

As discussed earlier, the dual-fuel combustion concept is a viable option to face the challenges of CI engines. Long ignition delay times promote more homogeneous mixture, which can lead, in combination with well-phased combustion, to high thermal efficiency with simultaneous low engine-out emissions.[36] In CI engines, the start of combustion depends on the injection time as well as on the ignition delay time. The ignition delay time mainly depends on the reaction kinetics of diesel fuel, which is very sensitive to small changes in quantities, such as intake temperature, intake pressure, and composition of the cylinder charge. Feedback control based on measured in-cylinder pressure is one option to control combustion processes with consideration of such external disturbances.[37] A detailed description of the applied combustion control approach is given in the next section.

For maintaining stable dual-fuel operation for the considered load range under stationary and transient conditions with flexible SRs, it is essential to develop a combustion controller. It allows for simultaneous control of various variables like combustion phasing, load, peak cylinder pressure, and SR. Once a combustion controller is available, it can also be used for a fast and partially automated calibration process.[38] The classical engine parameterizing approach relies on open-loop measurements based on the variation of the

manipulated variables. This approach has the consequence that automated measurements are only conditionally possible, because the a priori transfer of the operation limits like misfire or knocking as constraints for the manipulated variables is not possible. This study was performed following a different approach. First, open-loop system identification measurements were performed. Second, based on these data, a combustion controller was developed and validated. After successful validation, the investigations were conducted with activated combustion controller.

A deep understanding of the in-cylinder process is required for engine design and combustion controller development. To investigate the impact of different input parameters like injection duration (duration of energizing, DOE, which correlates with the injected diesel mass), injection timing (start of energizing, SOE), and SR on the output parameters (i.e. IMEP$_{HP}$, CA50, engine-out emissions, and ringing intensity), numerous investigations were conducted. Experiments with variations in injection timings (15–55 °CA bTDC) and injected mass (0.16–0.32 kg/h) were carried out, while engine speed (2000 r/min), Φ_{Global} (0.625), and injection pressure (540 bar) were held constant. In Figure 2, the input and output parameters of the dual-fuel process are illustrated, while the investigated key parameters are highlighted in green. Table 4 summarizes operation conditions of the performed experiments.

In this work, the following definitions for SR and Φ_{Global} were used, with H$_{u,i}$ as net heating value and AFR$_{st,i}$ as the stoichiometric air requirement

$$SR = \frac{\dot{m}_{CH_4} \cdot LHV_{CH_4}}{\dot{m}_{CH_4} \cdot LHV_{CH_4} + \dot{m}_{Diesel} \cdot LHV_{Diesel}} \quad (1)$$

$$\Phi_{Global} = \frac{\dot{m}_{CH4} \cdot AFR_{st,CH4} + \dot{m}_{Diesel} \cdot AFR_{st,Diesel}}{\dot{m}_{Air}} \quad (2)$$

For detailed thermodynamic analysis, the HRR is calculated from the indicated data[39] as

$$dQ_B = \frac{\kappa}{\kappa - 1} \cdot p \cdot dV + \frac{1}{\kappa - 1} \cdot V \cdot dp + dQ_W \quad (3)$$
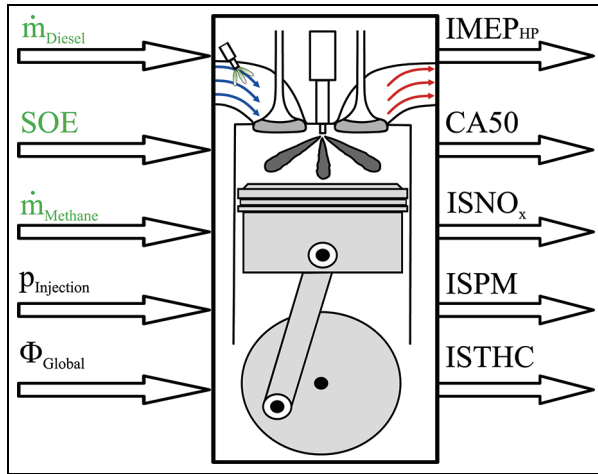
Figure 2. Investigated DDF key parameters.

Table 4. DDF operation conditions.

Quantity	Lower bound	Upper bound	Unit
Speed	2000	2000	r/min
CA50	−1	14	°CA aTDC
SOE	55	15	°CA bTDC
SR	70	90	%
Φ_{Global}	0.625	0.625	–
m_{Diesel}	0.16	0.32	kg/h
$\mathrm{m}_{Methane}$	1.0	1.0	kg/h
p_{Intake}	1.25	1.65	bar
$p_{Injection}$	540	540	bar
$p_{Exhaust}$	1.2	1.2	bar
T_{Intake}	316	316	K
$T_{Oil,\ Coolant}$	353	353	K

SOE: start of energizing; SR: substitution rate; aTDC: after top dead center; bTDC: before top dead center.

where p is cylinder pressure, V is cylinder volume, κ is isentropic coefficient, and dQ_W is wall heat losses.

The isentropic coefficient is calculated with NASA polynomials depending on gas composition and in-cylinder temperature.[40] Moreover, the correlation of Woschni is used for determining the wall heat losses.[39] Further analysis is performed to separate losses of the combustion process into incomplete combustion and non-ideal combustion. Incomplete combustion is calculated using combustion efficiency (η_C). For this, the net heating values of CO and THC emissions are computed, m_i are mass fractions of CO and THC, and compared to the energy of the fuel, $\dot{m}_f$ refers to the mass flow rate of the fuel

$$\eta_C = 1 - \frac{\sum\limits_{i=1}^{n} m_i \cdot LHV_i}{\dot{m}_f \cdot LHV_f} \qquad (4)$$

Finally, the results are compared to the limited-pressure cycle with maximum pressure at the load limit of the engine (150 bar) to account for losses associated with non-ideal combustion process.

Model-based dual-fuel control concept

From a control point of view, natural gas-diesel dual-fuel engines possess challenging properties, which must be considered and specifically addressed during the control design process. These are primarily:

- Strongly coupled multiple-input multiple-output system characteristics with a high number of variabilities due to the use of two fuel paths;
- Different time scales of the air, gas, and diesel fuel paths, which must be considered, especially during transient operation;
- Highly non-linear transfer behavior for the combustion process itself, specifically the influence of the diesel injection at different operating conditions on the combustion phasing.

Figure 5 shows the measured dependency of the center of combustion (CA50) from the injection timing of the diesel injection, set by the SOE, for different settings of the injected diesel fuel mass ($\dot{m}_{Diesel}$) with the injected gas fuel mass ($\dot{m}_{Methane}$) and the global equivalence-ratio (Φ_{Global}) being constant for all operating points. Characteristic for dual-fuel operation is the non-monotonic shape of the curves (SOE sweeps for different diesel fuel masses), which results in a sign-inversion of the static transfer coefficient from SOE to CA50, that is, of the static local sensitivity $\partial CA50/\partial SOE$.[22,37] Besides the injection timing, the injected fuel mass of the diesel injection has a strong influence on CA50. However, unlike the injection timing, its effect is strictly monotonic, that is, by increasing the diesel mass while keeping all other operating parameters constant, CA50 is always advanced to earlier timings. This results in a static local sensitivity ($\partial CA50/\partial \dot{m}_{Diesel}$) < 0. The knowledge of the static local sensitivities of the diesel fuel path with respect to the center of combustion ($\partial CA50/\partial SOE$, $\partial CA50/\partial \dot{m}_{Diesel}$) at every operating point or at least in dependence of the main influencing variables is essential for the design of the CA50 control loop. Using a model-based control approach, this information on the operating point dependent transfer behavior is used explicitly in terms of a controller-internal prediction model for the calculation of the manipulated variables.

Figure 3 gives a schematic overview of the modular, model-based dual-fuel control concept. The inputs of the control structure comprised set points for the main parameters defining the operating point of the engine (IMEP, SR, CA50, combustion mode, Φ_{Global}, $p_{Injection}$) and sensor data from various sensors, which are fed to the central combustion observer. The combustion observer provides online estimates of states and parameters and consists of different open and closed-loop observers. The final output of the controller are actuation signals for different components of the fuel and air path, for example, DOE and SOE, which are calculated in the component control loops (controllers for boost
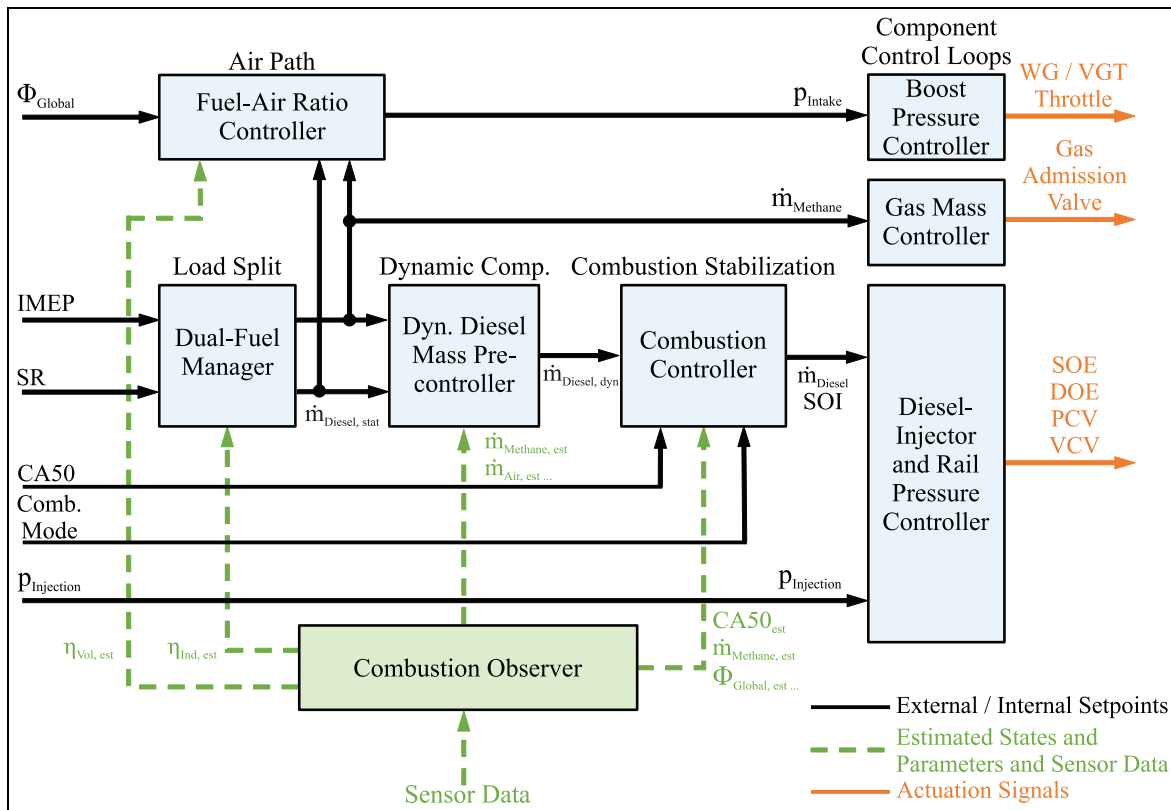
Figure 3. Overall control structure.

pressure, gas mass, and diesel injection). In between are functional blocks composing appropriate internal set points for the component control loops. In the following, a short description of the main functional blocks is given.

In the dual-fuel manager, the energetic load split is performed such that the internal set points for both fuel mass flows ($\dot{m}_{Methane}$, $m_{Diesel, stat}$) are calculated based on the desired load and diesel SR. The estimated indicated efficiency ($\eta_{Ind, est}$) from the combustion observer provides process feedback. The fuel mass flow set points are handed to the fuel-air ratio controller, which calculates the required boost pressure based on the estimated volumetric efficiency ($\eta_{Vol, est}$). Both fuel mass set points also serve as inputs for the dynamic diesel mass pre-controller that compensates the slow dynamics of the gas path by adjusting the diesel mass ($\dot{m}_{Diesel, dyn}$).

The key element of the control structure is the combustion controller, which has two objectives. The primary control objective is the stabilization of the CA50 close to its set point for the desired combustion mode and guarantees stable combustion, thus preventing abnormal combustion phenomena like knocking or misfire. The secondary control objective is the tracking of the desired diesel SR at stationary and of the load requirement (IMEP) at stationary as well as transient operation. For achieving both control objectives, the combustion controller can adjust injection timing and injected diesel fuel mass. For the tracking of CA50, it is necessary to use both variables because of the non-linear dependency between CA50 and SOE. Otherwise, local controllability of the process cannot be

guaranteed for every operating point. By using only the injection timing (SOI) as manipulated variable, controllability will be lost if the local sensitivity ($\partial CA50/\partial SOE$) approaches zero (cf. Figure 5).

Structurally, the combustion controller consists of a feedforward and a feedback path. The feedforward path can be regarded as a pre-controller, which is based on an optimization-based inversion of a non-linear data-based combustion model. This optimization is performed offline and therefore does not consider disturbances and model mismatch. This pre-controller provides injection timing as additional, internal set point for the feedback controller. The feedback controller is realized as a linear time-varying model predictive controller (MPC) with one-step prediction based on a successive linearization of the non-linear data-based combustion model, which was also used for designing the pre-controller. For compensation of disturbances and model mismatch and achieving offset-free reference tracking in stationary operation, the affine prediction model is augmented by an additional disturbance state. Figure 4 shows an experimental validation of the model-based dual-fuel control concept at quasi-stationary operation conditions with constant set points for IMEP, CA50, and Φ_{Global} and a time-varying quasi-stationary set point trajectory for SR. The controller is able to track all controlled variables independently of each other and offset-free to their corresponding set points for both combustion modes by manipulating both fuel masses, the injection timing of the diesel injection, and the boost pressure.
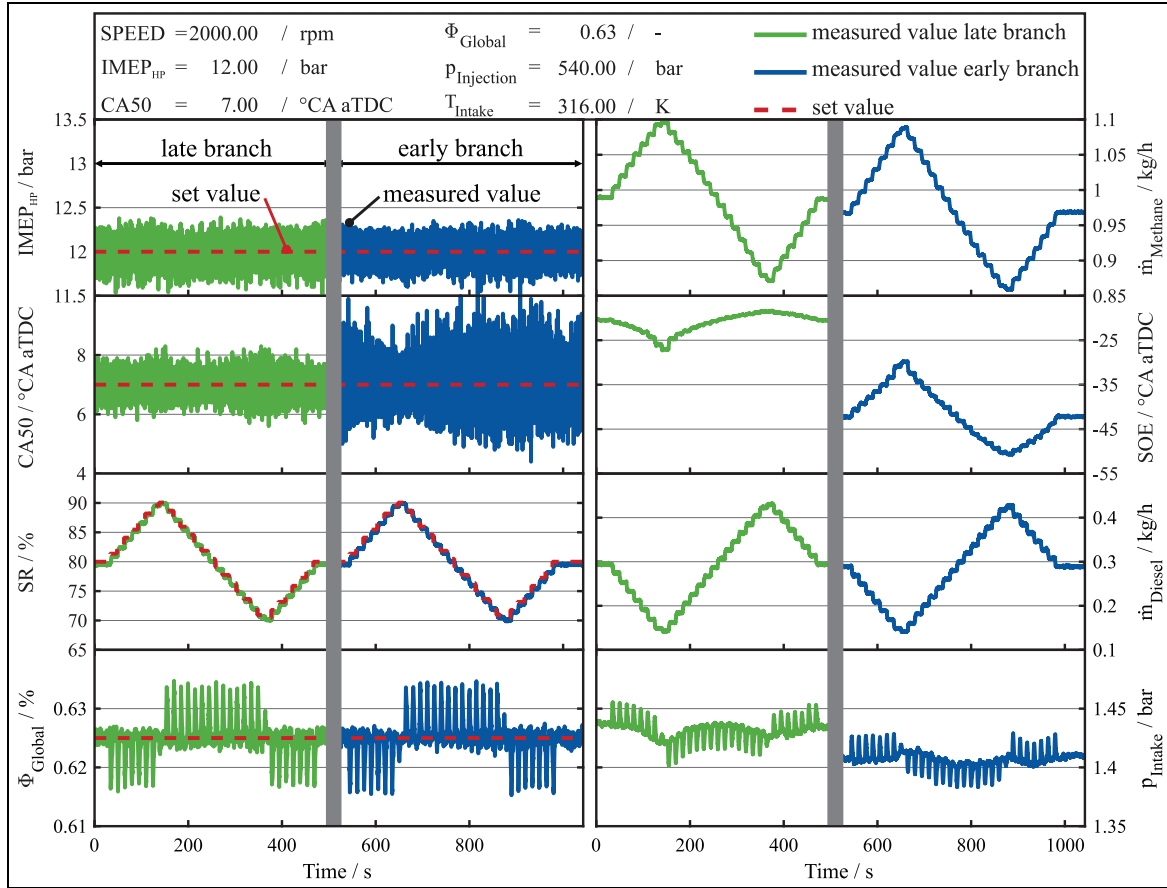
Figure 4. Combustion controller validation at quasi-stationary operation for constant Φ_{Global}, IMEP$_{HP}$ and CA50.

Experimental results

In this section, the experimental results are presented in the following order:

- Open-loop system identification measurements:
  CA50 in dependency of injection timing (SOE) and injection duration of diesel fuel (DOE) at constant operation conditions.
- Comparison of different combustion modes:
  Evaluation of performance and emissions metrics for late and early branches.
- Closed-loop measurements:
  Combustion controller results for stationary engine operation.

Non-linear characteristics of CA50 (open-loop measurements)

Figure 5 shows the results for sweeps in SOE and SR on CA50. Starting at 15 °CA bTDC, the SOE is advanced up to 55 °CA bTDC with an increment of 3 °CA, while SR is changed by decreasing the amount of diesel fuel from 0.32 to 0.16 kg/h. Engine speed, Φ_{Global}, injection pressure, and mass flow of methane are held constant. Operation conditions are summarized in Table 4.
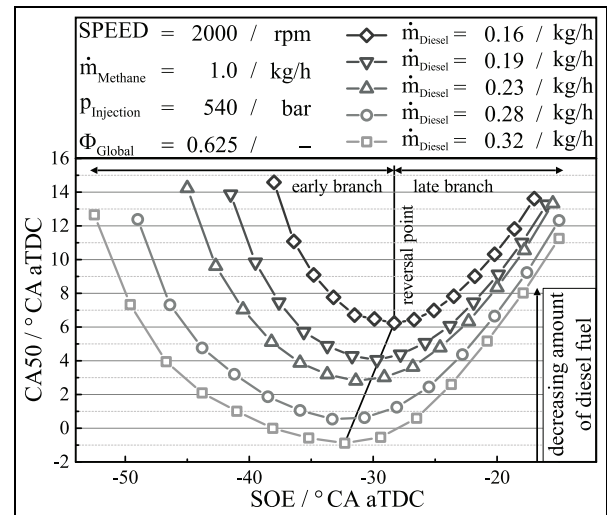

Figure 5. CA50 as a function of SOE sweep for different amounts of diesel fuel at constant speed, Φ_{Global}, p$_{Injection}$, and ṁ$_{Methane}$.

From Figure 5, different dependencies between CA50 and SOE, and between CA50 and the injected amount of diesel fuel are observed. Based on these dependencies, the curves are divided into three areas. The process characteristics are described for the 0.32 kg/h case.

For the interval from $-15\,°CA$ aTDC to $-30\,°CA$ aTDC, $(\partial CA50/\partial SOE) > 0$, that is, an advancement of SOE leads to an advancement of CA50. This area is referred to as late branch and is designated with injection timings close to TDC. For further advancement of SOE, $(\partial CA50/\partial SOE) = 0$, due to the occurrence of a reversal point, which is characterized by the earliest CA50, that is, $-1\,°CA$ aTDC. For injection timings beyond the reversal point, that is, earlier than $-35\,°CA$ aTDC, combustion is delayed and a sign-inversion of the local sensitivity, that is, $(\partial CA50/\partial SOE) < 0$, is observed. This area is referred to as early branch (cf. Figure 5).

The fact that for the early branch, CA50 is retarded despite earlier SOE can be explained by considering the interaction of chemical and mixing time scales. If the diesel fuel is injected early in the compression stroke, the chemical time scales are relatively long and hence more time is available for mixing. The local fuel/air mixture becomes leaner, and lean mixtures have longer ignition delay time, which might be the reason for retarding CA50.[41] Moreover, the ignition mode for diesel fuel is changed for the early injection timings. While in CDC injection timing of diesel fuel is essential for the start of combustion, mixture formation, pressure, and temperature are more important than the injection timing during the two-stage ignition mode.[42] Similar trends between CA50 and injection timing have been reported by other researchers.[25,26,42–44]

The described dependencies can be observed for all SR considered in this study (cf. Figure 5). However, the CA50 shifts toward later timings with decreasing diesel mass and the position of the earliest CA50 moves toward later injection timings, which is related to the reduced time to promote a lean mixture. Moreover, the influence of the injection timing is weaker for smaller amounts of diesel, that is, the absolute change in CA50 decreases. Based on the data shown in Figure 5, it can be concluded that the amount of injected diesel fuel has a monotonic influence on combustion, which leads to advanced CA50 by increasing DOE.

To summarize, the CA50 dependency on SOE is characterized by a non-linear behavior with an early ignition and a late ignition branch. In addition, it is noteworthy that the injected amount of diesel fuel has a strong effect on the sensitivity of CA50 on SOE during the early branch, that is, decreasing amounts of diesel fuel lead to a steeper rise in the CA50, while the changes in the slope of the late branch are smaller. From Figure 5, it is evident that the same CA50 value can be achieved with two different injection strategies, that is, early or late branch.

Comparison of performance and emissions metrics for different combustion modes

In order to assess the different branches, some selected performance and emissions metrics including ISNO$_x$ (a), ISTHC (b), ISPM (c), and the indicated efficiency (dashed lines) are illustrated in Figure 6. Emissions are shown as surface plots, while iso-lines are used for the efficiency.

As shown in Figure 6, the indicated efficiency is influenced by SOE and SR, where SOE shows a stronger impact. Regions of high efficiency are achieved at low SR (here, 76%) and on the early branch (CA50 close TDC). Moreover, the change in indicated efficiency due to SOE on the late branch is higher than on the early branch. On the early branch, the indicated efficiency is mainly influenced by the SR. ISTHC emissions reach a maximum on the late branch and for retarded CA50, while lowest emissions are obtained on the early branch and with advanced CA50. Increasing ISTHC emissions can be associated with the decreased combustion temperature, which leads to more severe flame quenching at the combustion chamber walls. The development of the ISTHC emissions is in line with the indicated efficiency.

For the ISNO$_x$ emissions, the highest values are observed for CA50 close to TDC and lowest for retarded CA50 and contrary to ISTHC emissions development, which is in accordance with the combustion temperature. ISPM emissions are influenced by the SOE and SR, that is, lowest soot emissions are observed for highest SR and on the late branch, while low SR and early injection timings lead to the highest soot emissions, which can be attributed to early injection timings. Low density and cooler bulk gases in the combustion chamber enhance the penetration length of the diesel spray, which could lead to wall wetting. These observations can be explained by effects like the reduction of diesel fuel quantity, that is, reduction of diffusive combustion since CDC is associated with high soot emissions. Furthermore, the combination of increased ignition delay time to promote a homogeneous mixture and the reduced combustion temperature constrain soot formation.[3,32]

To summarize, regions with high efficiency and low emissions are revealed. For further reduction of emissions, that is, ultra-low NO$_x$ and soot, different strategies like EGR, multiple-injection strategy, and higher injection pressure can be applied.

Figure 7 illustrates in-cylinder and performance data at constant speed (2000 r/min), $p_{Injection}$ (540 bar), Φ_{Global} (0.625), SR (82%), and approximately the same IMEP$_{HP}$ as well as CA50 (cf. Figure 6, stars). Performance metrics, pressure trace, injector current, HRR, and the total heat release are shown for the late and early branches.

For the late injection timing, lower maximum cylinder pressure, higher pressure rise rate, retarded start of combustion, and an extended duration of the combustion process are recorded. In contrast to late injection timings, higher cylinder pressure, reduced pressure rise rate, earlier start of combustion, and shortened combustion duration are measured for the early injection timing. From HRR analysis, different combustion
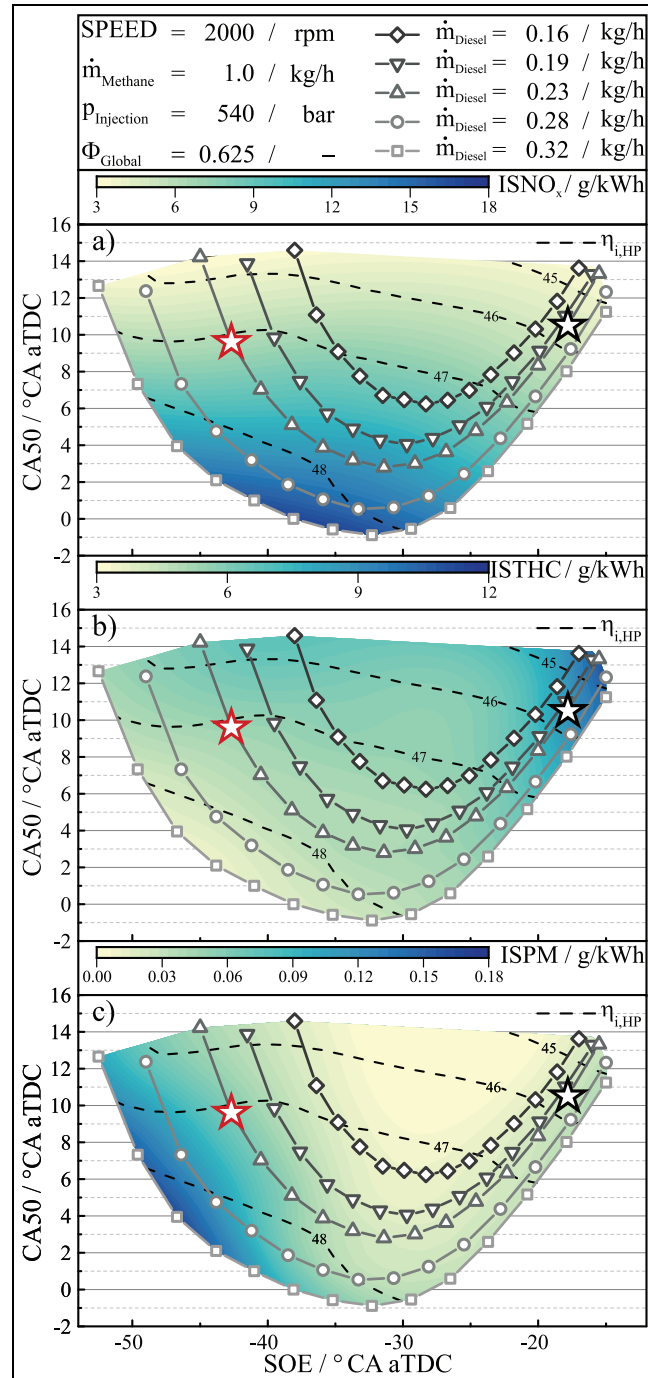
Figure 6. Selected performance and emissions metrics for CA50 as function of SOE for different SR including (a) ISNO$_x$, (b) ISTHC, and (c) ISPM, with iso-lines for the indicated efficiency (dashed lines). Comparable CA50 for late and early branch is highlighted with stars.

regimes can be identified. For the late injection timing, the rapid heat release due to partially premixed diesel combustion is clearly visible, followed by flame propagation through the methane-air mixture. The HRR for the early injection timing is very smooth and different combustion regimes are no longer visible. This indicates the combustion of a more homogenized diesel-methane-air mixture with predominantly premixed combustion. In terms of performance as well as engine-

out emissions, benefits for the early injection timing are observed, such as significant reduction in ISTHC and RI. However, a slight increase in ISPM and ISNO$_x$ emissions was noticed. Furthermore, an increase in IMEP$_{HP}$ and in indicated efficiency was detected (cf. Figure 7).

To investigate the increase in indicated efficiency for the early injection case compared to the late injection operating conditions, thermodynamic considerations
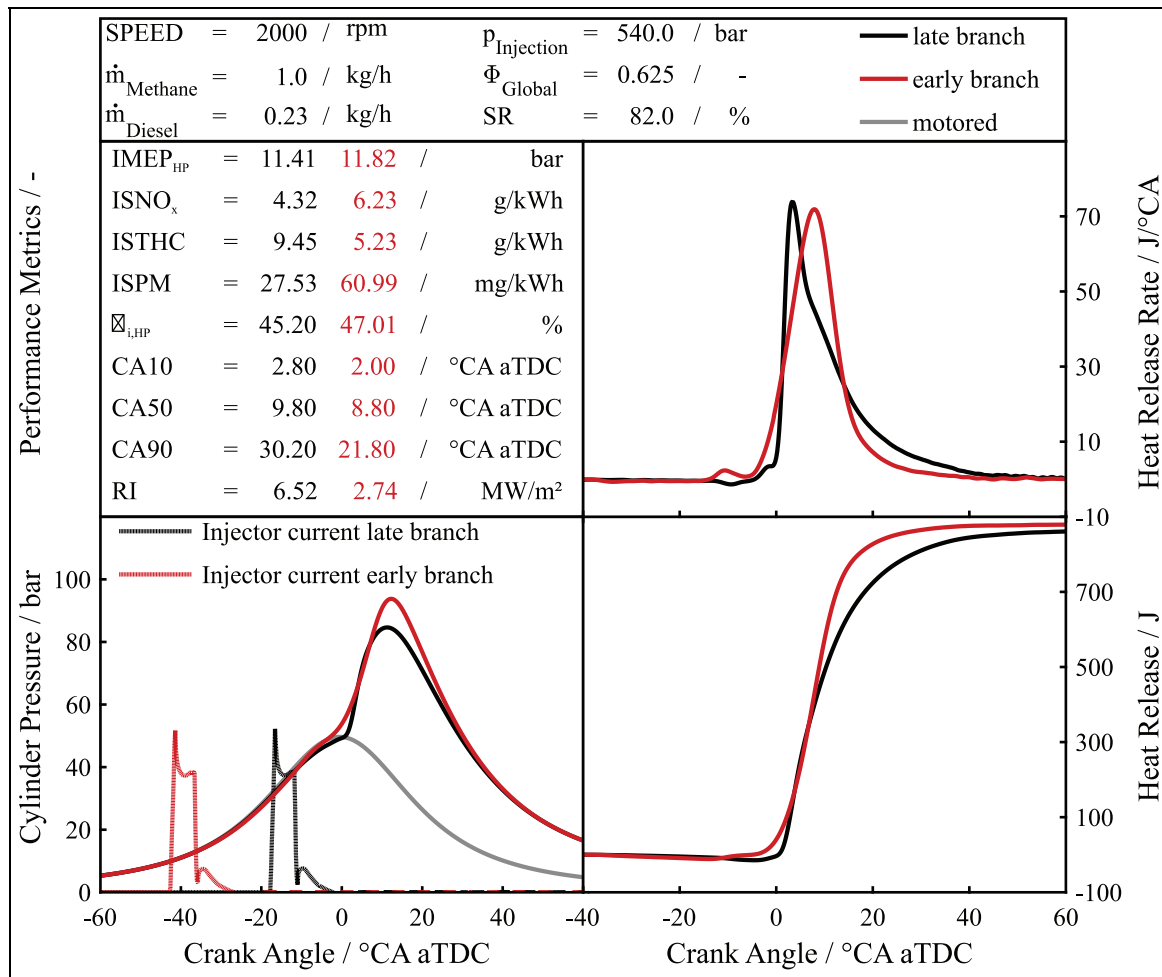
Figure 7. In-cylinder data, that is, cylinder pressure, injector current, HRR, and HR, for comparable CA50 and IMEP for early and late branch. In addition, performance and engine-out emissions metrics are shown.
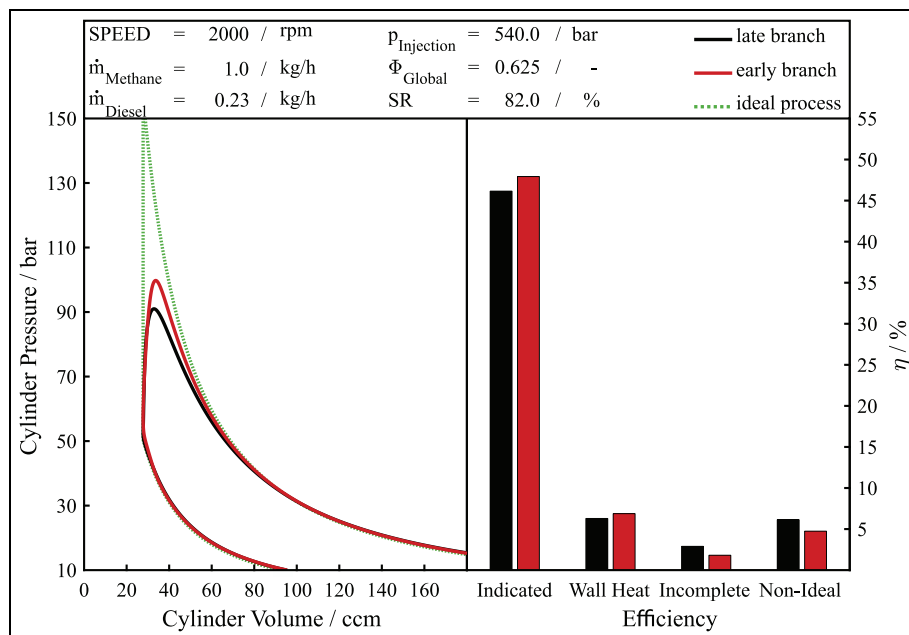

Figure 8. Partition of losses for both injection timings. Engine losses are shown as p-V-diagram (left) and as bar charts (right).

are used to identify the driving mechanisms. Using the measured in-cylinder pressure as baseline, computations were performed to calculate losses due to incomplete combustion, wall heat transfer, and non-ideal combustion, which describes the deviation of the heat release curve from isochoric/isobaric heat supply and was determined via the analysis of the pressure trace. The results are illustrated in Figure 8 as p-V-diagrams (left) and as bar charts (right). This analysis shows that the early injection case suffers much less from incomplete combustion and non-ideal combustion effects. The slightly increased wall heat transfer is due to the higher maximum pressure and thus increased combustion temperatures. The incomplete combustion for the late injection case indicates that the partially premixed diesel combustion and the ensuing premixed methane-air combustion achieve temperatures that prevent complete burn-out of the end-gases. On the contrary, the improved premixing for the early injection case results in combustion temperatures sufficiently high for a flame propagating through almost the whole volume of the cylinder. In this way, the combustion process comes also closer to the limited-pressure cycle.

Combustion controller results for stationary engine operation (closed-loop measurements)

Using the developed combustion controller, the impact of injection timing and SR on performance and emissions metrics was studied for constant operation conditions. Engine speed, $IMEP_{HP}$, Φ_{Global} (0.555), and $p_{Injection}$ were held constant, while sweeps in CA50 and SR were performed. CA50 was varied between 1 °CA aTDC and 13 °CA aTDC with an increment of 1 °CA, for both the late and the early branches. The measurements were repeated for all SR levels from 70% to 90%.

In Figure 9, emissions data are shown in terms of $ISNO_x$ (a), ISTHC (b), and ISPM (c). Moreover, iso-lines for the indicated efficiency and the TIER IMO 3 emission limits (blue designated area) are illustrated. While it is evident that the combustion controller is able to adjust the desired $IMEP_{HP}$, CA50, and SR simultaneously for both combustion modes, some combinations of CA50 and SR are infeasible. For example, the reversal point is achieved only for the highest SR, while the latest CA50 is only possible for SR = 85% and early injection timings. Furthermore, the interval of CA50 is decreasing with increasing SR. These differences were attributed to model prediction errors as the MPC was developed and validated for a higher Φ_{Global}.

Overall, the decrease in Φ_{Global} leads to a significant reduction in $ISNO_x$ emissions and enables compliance with the emissions limits. Moreover, with the use of the combustion controller, the required test bench time was significantly reduced.
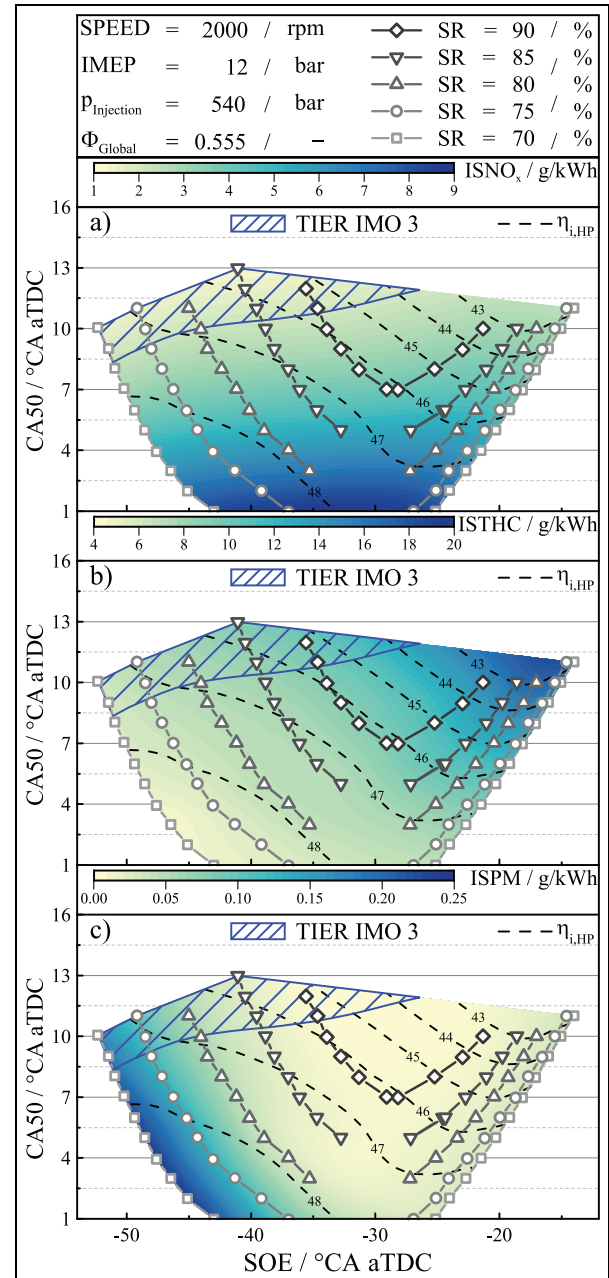

Figure 9. Selected performance and emissions metrics for CA50 as function of SOE for different SR including (a) $ISNO_x$, (b) ISTHC, and (c) ISPM, with iso-lines for the indicated efficiency (black dashed lines) and TIER IMO 3 emissions limits, which only consider $ISNO_x$ emissions (blue designated area).

Conclusion

In this work, an experimental investigation of dual-fuel combustion was carried out, studying the impact on engine-out emissions and performance metrics in a CI engine. In the experiments, a premixed methane/air mixture and direct injection of diesel fuel were utilized. Variations in injection timings, injected fuel mass, and SRs were conducted and evaluated. The experiments revealed different dependencies between injection

timing and combustion phasing. For injection timings close to TDC, a linear dependency was observed with earlier CA50 for earlier SOE, while for further advanced injection timings a reversal point in CA50 was detected. For even earlier SOE, the combustion was again retarded, which was found to originate from the locally leaner mixtures. Besides, different levels of emissions were obtained for varying injection timings. For a deeper understanding of the combustion modes, a detailed analysis of the in-cylinder processes was carried out. It was shown that the early injection timings in combination with lean air-fuel mixtures reduce the losses from incomplete combustion (ISTHC) and non-ideal combustion process, which led to an increase in thermal efficiency. Based on these system identification measurements, a model predictive combustion controller was developed and validated. Finally, it was demonstrated that the developed combustion controller was able to adjust simultaneously the desired load, combustion phasing, and SR for different combustion modes. Overall, this study shows that DDF operation in combination with a sophisticated combustion controller is a promising concept to counteract the drawbacks of CI engines and to comply with legislative emissions limits (TIER IMO 3).

Declaration of conflicting interests

The author(s) declared no potential conflicts of interest with respect to the research, authorship, and/or publication of this article.

ORCID iD

Metin Korkmaz https://orcid.org/0000-0002-4552-118X

References

1. Heywood JB. *Internal combustion engine fundamentals*, Vol. 21. New York: McGraw-Hill International, 1988, p.930.
2. Stone R. *Introduction to internal combustion engines*. London: Macmillan Education, 1992.
3. Akihama K, Takatori Y, Inagaki K, Sasaki S and Dean AM. Mechanism of the smokeless rich diesel combustion by reducing temperature. SAE technical paper 2001-01-0655, 2001.
4. Wissink M and Reitz R. Exploring the role of reactivity gradients in direct dual fuel stratification. *SAE Int J Engines* 2016; 92(2): 1036–1048.
5. Nieman DE, Dempsey AB and Reitz RD. Heavy-duty RCCI operation using natural gas and diesel. *SAE Int J Engines* 2012; 5(2): 270–285.
6. Splitter D, Wissink M, Kokjohn S and Reitz RD. Effect of compression ratio and piston geometry on RCCI load limits and efficiency. SAE technical paper 2012-01-0383, 2012.
7. Wissink M and Reitz R. The role of the diffusion-limited injection in direct dual fuel stratification. *Int J Engine Res* 2017; 18(4): 351–365.
8. Neely GD, Sasaki S, Huang Y, Leet JA and Stewart DW. New diesel emission control strategy to meet US tier 2 emissions regulations. SAE technical paper 2005-01-1091, 2005.
9. Musculus MPB, Miles PC and Pickett LM. Conceptual models for partially premixed low-temperature diesel combustion. *Prog Energ Combust Sci* 2013; 39(2–3): 246–283.
10. Paykani A, Kakaee AH, Rahnama P and Reitz RD. Progress and recent trends in reactivity-controlled compression ignition engines. *Int J Engine Res* 2016; 17(5): 481–524.
11. Reitz RD. Directions in internal combustion engine research. *Combust Flame* 2013; 160(1): 1–8.
12. Dec JE. Advanced compression-ignition engines—understanding the in-cylinder processes. *Proc Combust Inst* 2009; 32(2): 2727–2742.
13. Papagiannakis RG, Rakopoulos CD, Hountalas DT and Rakopoulos DC. Emission characteristics of high speed, dual fuel, compression ignition engine operating in a wide range of natural gas/diesel fuel proportions. *Fuel* 2010; 89(7): 1397–1406.
14. Wei L and Geng P. A review on natural gas/diesel dual fuel combustion, emissions and performance. *Fuel Proc Technol* 2016; 142: 264–278.
15. Korakianitis T, Namasivayam AM and Crookes RJ. Natural-gas fueled spark-ignition (SI) and compression-ignition (CI) engine performance and emissions. *Prog Energ Combust Sci* 2011; 37(1): 89–112.
16. Splitter D, Wissink M, DelVescovo D and Reitz RD. RCCI engine operation towards 60% thermal efficiency. SAE technical paper 2013-01-0279, 2013.
17. Splitter D, Hanson R, Kokjohn S, Wissink M and Reitz RD. Injection effects in low load RCCI dual-fuel combustion. SAE technical paper 2011-24-0047, 2011.
18. Kokjohn SL, Hanson RM, Splitter DA and Reitz RD. Experiments and modeling of dual-fuel HCCI and PCCI combustion using in-cylinder fuel blending. *SAE Int J Engines* 2010; 2(2): 24–39.
19. Königsson F, Stalhammar P and Angstrom HE. Characterization and potential of dual fuel combustion in a modern diesel engine. SAE technical paper 2011-01-2223, 2011.
20. Selim MYE. Sensitivity of dual fuel engine combustion and knocking limits to gaseous fuel composition. *Energ Convers Manage* 2004; 45(3): 411–425.
21. Hanson R, Kokjohn S, Splitter D and Reitz RD. Fuel effects on reactivity controlled compression ignition

(RCCI) combustion at low load. *SAE Int J Engines* 2011; 4(1): 394–411.

22. Königsson F, Stalhammar P and Ångström HE. Combustion modes in a diesel-CNG dual fuel engine. SAE technical paper 2011-01-1962, 2011.

23. Königsson F, Kuyper J, Stalhammar P and Ångström HE. The influence of crevices on hydrocarbon emissions from a diesel-methane dual fuel engine. *SAE Int J Engines* 2013; 6(2): 751–765.

24. Inagaki K, Mizuta J, Fuyuto T, Hashizume T, Ito H, Kuzuyama H, et al. Low emissions and high-efficiency diesel combustion using highly dispersed spray with restricted in-cylinder swirl and squish flows. *SAE Int J Engines* 2011; 4(1): 2065–2079.

25. DelVescovo D, Kokjohn S and Reitz R. The effects of charge preparation, fuel stratification, and premixed fuel chemistry on reactivity controlled compression ignition (RCCI) combustion. *SAE Int J Engines* 2017; 10(4): 1491–1505.

26. Roberts G, Rousselle CM, Musculus M, Wissink M, Curran S and Eagle E. RCCI combustion regime transitions in a single-cylinder optical engine and a multi-cylinder metal engine. *SAE Int J Engines* 2017; 10(5): 2392–2413.

27. Reitz RD and Duraisamy G. Review of high efficiency and clean reactivity controlled compression ignition (RCCI) combustion in internal combustion engines. *Prog Energ Combust Sci* 2015; 46: 12–71.

28. Huang J and Crookes RJ. Assessment of simulated biogas as a fuel for the spark ignition engine. *Fuel* 1998; 77(15): 1793–1801.

29. Krishnan SR, Srinivasan KK, Singh S, Bell SR, Midkiff KC, Gong W, et al. Strategies for reduced NOx emissions in pilot-ignited natural gas engines. *J Eng Gas Turbines Power* 2004; 126(3): 665–671.

30. Papagiannakis RG and Hountalas DT. Combustion and exhaust emission characteristics of a dual fuel compression ignition engine operated with pilot diesel fuel and natural gas. *Energ Convers Manage* 2004; 45(18–19): 2971–2987.

31. Imran S, Emberson DR, Diez A, Wen DS, Crookes RJ and Korakianitis T. Natural gas fueled compression ignition engine performance and emissions maps with diesel and RME pilot fuels. *Appl Therm Eng* 2014; 67(1–2): 354–365.

32. Yu S, Gao T, Wang M, Li L and Zheng M. Ignition control for liquid dual-fuel combustion in compression ignition engines. *Fuel* 2017; 197: 583–595.

33. Srinivasan KK, Krishnan SR and Midkiff KC. Improving low load combustion, stability, and emissions in pilot-ignited natural gas engines. *Proc IMechE, Part D: J Automobile Engineering* 2006; 220(2): 229–239.

34. Zhou L, Liu YF, Wu CB, Sun L, Wang L, Zeng K and Huang ZH. Effect of the diesel injection timing and the pilot quantity on the combustion characteristics and the fine-particle emissions in a micro-diesel pilot-ignited natural-gas engine. *Proc IMechE, Part D: J Automobile Engineering* 2013; 227(8): 1142–1152.

35. Yang B, Xi C, Wei X, Zeng K and Lai MC. Parametric investigation of natural gas port injection and diesel pilot injection on the combustion and emissions of a turbocharged common rail dual-fuel engine at low load. *Appl Energ* 2015; 143: 130–137.

36. Ingesson G, Yin L, Johansson R and Tunestal P. Simultaneous control of combustion timing and ignition delay in multi-cylinder partially premixed combustion. *SAE Int J Engines* 2015; 8(5): 2089–2098.

37. Ott T, Zurbriggen F, Onder C and Guzzella L. Cylinder individual feedback control of combustion in a dual fuel engine. *IFAC Proc Vol* 2013; 46(21): 600–605.

38. Asprion J, Chinellato O and Guzzella L. Optimal control of diesel engines: numerical methods, applications, and experimental validation. *Math Probl Eng* 2014; 2014(1): 286538.

39. Pischinger R, Klell M and Sams T. *Thermodynamik der Verbrennungskraftmaschine*, vol. 29.1. Vienna: Springer, 2010, pp.53–61.

40. McBride BJ, Sanford G and Martin AR. *Coefficients for calculating thermodynamic and transport properties of individual species* (NASA-TM-4513). Washington, DC: National Aeronautics and Space Administration (NASA), 1993, p.96.

41. Warnatz J, Maas U and Dibble RW. *Combustion*. Berlin: Springer, 2006.

42. Wang Z, Zhao Z, Wang D, Tan M, Han Y, Liu Z and Dou H. Impact of pilot diesel ignition mode on combustion and emissions characteristics of a diesel/natural gas dual fuel heavy-duty engine. *Fuel* 2016; 167: 248–256.

43. Eichmeier J, Wagner U and Spicher U. Controlling gasoline low temperature combustion by diesel micro pilot injection. *J Eng Gas Turbines Power* 2012; 134(7): 072802.

44. Ma S, Zheng Z, Liu H, Zhang Q and Yao M. Experimental investigation of the effects of diesel injection strategy on gasoline/diesel dual-fuel combustion. *Appl Energ* 2013; 109: 202–212.

Appendix I

Notation

AFR	air-fuel ratio
aTDC	after top dead center
bTDC	before top dead center
CA10	crank angle when 10% fuel is consumed
CA50	crank angle when 50% fuel is consumed
CA90	crank angle when 90% fuel is consumed
CD	combustion duration (CA90-CA10)
CDC	conventional diesel combustion
CI	compression ignition
CLD	chemiluminescence detection
CNG	compressed natural gas
CO	carbon monoxide
CO_2	carbon dioxide
DDF	diesel-dual fuel
DOE	duration of energizing
ECU	engine control unit
EGR	exhaust gas recirculation
FBP	final boiling point
FID	flame ionization detector
HRR	heat release rate
IMEP	indicated mean effective pressure
ISFC	indicated specific fuel consumption
$ISNO_x$	indicated specific amount of NO_x
ISPM	indicated specific particulate matter
ISTHC	indicated specific amount of total hydrocarbons
LHV	lower heating value

LPG	liquefied petroleum gas	RPM	revolutions per minute
LTC	low-temperature combustion	SOE	start of energizing
MIMO	multi-input multi-output	SR	substitution rate
MPC	model predictive control	TDC	top dead center
PFI	port fuel injection	TRA	thermodynamic real-time analysis
$p_{Injection}$	injection pressure		
p_{Intake}	intake pressure	η_C	combustion efficiency
PPRR	peak pressure rise rate	$\eta_{i,\,HP}$	indicated efficiency of the high-pressure loop
RCCI	reactivity controlled compression ignition		
RCP	rapid control prototyping	Φ	fuel-air equivalence ratio
RI	ringing intensity		